International Journal of Engineering

Journal Homepage: www.ije.ir

Lateral Load Carrying Capacity of Concrete-filled Cold-formed Steel Shear Wall

G. Sijwal[a], P. Man Pradhan[b,c], K. Phuvoravan*[a]

[a] *Department of Civil Engineering, Faculty of Engineering, Kasetsart University, Bangkok, Thailand*
[b] *Department of Civil Engineering, School of Engineering, Kathmandu University, Dhulikhel, Nepal*
[c] *School of Engineering, Manmohan Technical University, Morang, Nepal*

PAPER INFO

Paper history:
Received 16 August 2021
Received in revised form 28 September 2021
Accepted 05 October 2021

Keywords:
Concrete-filled Cold-formed Steel Shear Wall
Monotonic Load
Experimental Investigation
Non-linear Finite Element Analysis
Parametric Studies

ABSTRACT

A new type of innovative composite shear wall, concrete-filled cold-formed steel shear wall (CFCSW) is proposed, composed of cold-formed channel sections arc-welded together by 20 mm length of welds and filled with concrete. The main study of CFCSW focuses on the overall behavior, ultimate load capacity, stiffness and ductility. Three specimens of CFCSW with an aspect ratio of 1.0 are tested under lateral monotonic load. Three-dimensional finite element models are developed and benchmarked with the experimental results. The validated models are used to carry out parametric studies to determine the influence of the parameters on the performance of the CFCSW. The parameters are the height, steel plate thickness, weld spacing and concrete thickness of the CFCSW. The experimental and finite element modeling results indicate that increasing the weld spacing from 105 mm to 211 mm improves the stiffness, ductility and load carrying capacity, and similarly, providing holes inside the wall increases the stiffness, ductility and peak strength of the CFCSW. The ultimate capacity of the CFCSW is the most influenced by changing the height of the wall and least influenced by varying the concrete thickness of the wall.

doi: *10.5829/ije.2022.35.01a.15*

1. INTRODUCTION

Generally, reinforced concrete shear walls are used in high-rise buildings. However, they present construction difficulties, which result in delays during construction and they have limitations when more strength and more ductility are required in shear walls [1-3]. Therefore, innovation in shear wall is necessary. Four types of wall have been suggested by past researchers as alternatives to the traditional reinforced concrete shear wall. The first is the steel plate shear wall, which can withstand large inelastic deformations [4-7]; however, local buckling in the compression zone of the steel plate greatly reduces the stiffness and strength capacity of the shear wall [8]. Using stiffeners and increasing the steel plate thickness can avoid the buckling problem, but it is considered uneconomical. The second type of shear wall is the composite wall, which consists of steel frame boundaries and a steel plate inside the concrete [9-12]. The third form consists of a steel plate embedded in the reinforced concrete shear wall [13-16]. The fourth form is a concrete wall sandwiched by two steel plates, called a double-skin composite shear wall [1, 17].

A considerable amount of research has been done on the double-skin plate composite wall. Initially, the in-plane shear behavior of a double-skin plate composite wall with boundary elements was discussed by Ozaki et al. [18]. Varma et al. [19] proposed and verified the simple mechanics-based model (MBM) for the walls with boundary elements. Furthermore, Booth et al. [20] investigated the ultimate in-plane shear strength of the steel-plate composite wall with boundary elements and found that it mainly depends on the yield strength of steel face plate and the diagonal compression capacity of the cracked infilled concrete. Epackachi et al. [21] tested four specimens, named steel-plate composite wall piers, consisting of studs and tie rods, and determined that the failure pattern of the wall is governed by flexure rather than by shear. Luo et al. [17] and Zhang et al. [2] examined the in-plane seismic behavior of the wall with

*Corresponding Author Institutional Email: fengkpp@ku.ac.th (K. Phuvoravan)

Please cite this article as: G. Sijwal, P. Man Pradhan, K. Phuvoravan, Lateral Load Carrying Capacity of Concrete-filled Cold-formed Steel Shear wall, ***International Journal of Engineering, Transactions A: Basics*** Vol. 35, No. 01, (2022) 161-171

vertical stiffeners and connectors under reversed cyclic lateral load and axial compressive load. Luo et al. [17] ex-perimentally studied the behavior of the shear wall by varying the aspect ratio (height to length), concrete strength, axial compression ratio and plate thickness and found that the arrangement of the wall best utilizes the steel and concrete strength. Zhang et al. [1], through experiments, concluded that the ductility of the wall is greatly influenced by the thickness of the shear wall and the number of channels in the wall [17].

The above-mentioned researches mainly focused on cyclic behavior of the walls with the use of connectors like studs and tie rods. Therefore, a new type of composite wall (CFCSW) was put forward for ease of construction without the connectors and composed of cold-formed lipped C-sections connected by flare V-groove welds and filled concrete. Only the in-plane monotonic load was considered. The behavior of the proposed wall was investigated through the experimental tests with regards to the stiffness, ductility, ultimate capacity and failure mechanism. Finite element analysis was conducted to predict the peak strength of the wall and validated using the test results. Finally, sensitivity analysis was carried out to investigate the influence of the height, steel plate thickness, weld spacing and concrete thickness.

2. EXPERIMENTAL PROGRAM

2. 1. Specimen Description In general, the shear walls used in the high-rise building have the thickness ranging from 300 mm to 1800 mm and the steel plate reinforcement ratio, described as $2t_p/T$, varying from 1.5%-5%, where t_p is the thickness of steel plate and T is the thickness of wall [1]. This experiment was to study the shear wall system in a high-rise building. Three 1:5 scale down CFCSW specimens were designed to represent the wall, which has the height, length and thickness of 4320 mm, 3570 mm and 510 mm, respectively. All three specimens had an aspect ratio of 1.0, where the aspect ratio is the ratio of the clear height (overall height minus loading steel plate height) to the length of the wall [1, 17]. The configurations of the three tested specimens are listed in Table 1. The details for the cross-section, elevation, and inner channel of the specimens are shown in Figures 1 to 5.

Initially, fourteen cold-formed steel channels were arranged as shown in Figure 1 and connected by the welds. The hollow steel wall thus formed was fillet-welded to the steel base plate of thickness 38 mm. Furthermore, shear studs were installed on the baseplate so that the concrete could transfer the load sufficiently to the baseplate. Overall, the strength of the connection between the baseplate and the wall was designed to resist the estimated ultimate load. Then, ready-mix concrete was used to cast the wall to make the concrete-filled cold-formed steel shear wall (CFCSW). Flare V-groove welds with a length of 20 mm were used for welding, which is the minimum length of weld according to American Structural Welding code [22]. Similarly, the weld spacing of 105 mm (one eighth of overall height, Figure 2) was chosen for CFCSW1 as per the AISI code [23], whereas the weld spacings for CFCSW2 and CFCSW3 were approximately double that of CFCSW1 (Figure 3). Additionally, square holes with the size of 80 mm x 80 mm were made in the web of the inner channel sections for CFCSW1 and CFCSW2 (Figure 4) based on the AISC guideline for castellated and cellular beam [24]. Therefore, the weld spacings and the holes in the inner webs are the fundamental parameters that were investigated in this experiment regarding their effect on the structural behavior of the wall.

TABLE 1. Configurations of test specimen

Specimen	Cross-section (mm x mm)	Center-center spacing of welds (mm)	Size of square holes (mm x mm)
CFCSW1	714 x 102	105	80 x 80
CFCSW2	714 x 102	211	80 x 80
CFCSW3	714 x 102	211	No holes

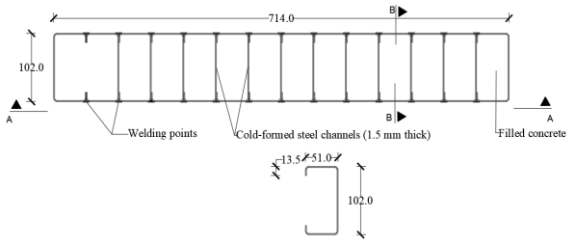

Figure 1. Typical cross-section of specimens and details of cold-formed channel section (units in mm)

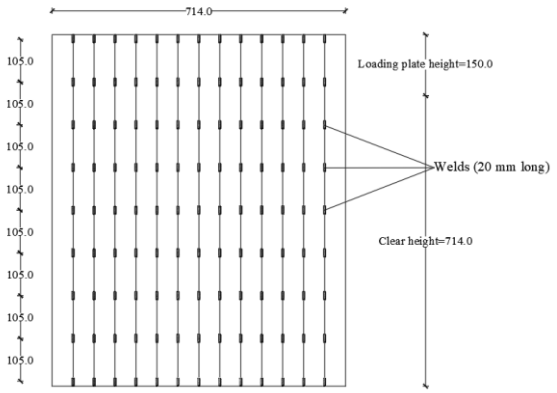

Figure 2. Elevation view A-A with welding details of CFCSW1 (units in mm)

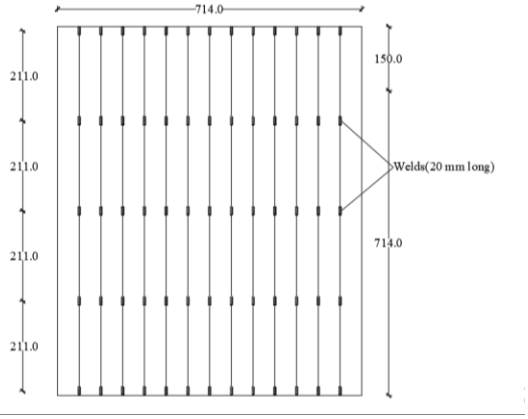

Figure 3. Elevation view A-A with welding details of CFCSW2 and CFCSW3 (units in mm)

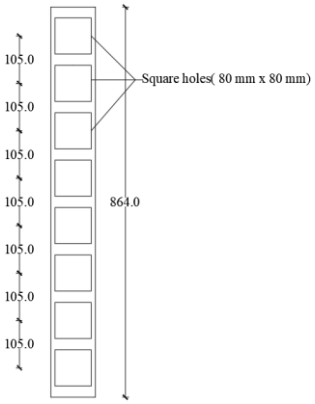

Figure 4. Details of holes in CFCSW1 and CFCSW2 (section B-B, units in mm)

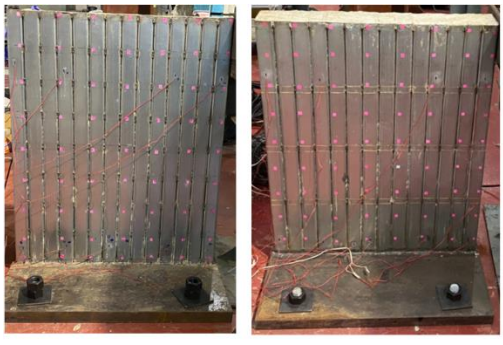

Figure 5. Specimens (a) CFCSW1 (b) CFCSW2 and CFCSW3

2. 2. Material Properties Three tensile coupon tests were carried out to determine the mechanical properties of the cold-formed steel. Young's modulus of elasticity, the yield and ultimate strength of the cold-formed steel obtained from the tests were 197.9 GPa, 463.9 MPa and 490.9 MPa, respectively. Likewise, the compressive strength of the concrete, calculated from the concrete cylinders at 28 days, was 21.0 MPa for all three specimens.

2. 3. Test Setup and Instrumentation The test setup used in the experiment is shown in Figures 6 and 7. The horizontal load, which was monotonic in nature, was applied using a hydraulic jack at the top of the wall via the loading plate. Eight nuts (50 mm outer diameter), four bolts (32 mm diameter) and four washer plates (25 mm thick) were used to attach the baseplate tightly to the concrete foundation block to prevent baseplate movement during the experiment. Displacement-controlled loading with a speed of approximately 0.048 mm/sec was implemented in the test. The test was terminated when the applied lateral load dropped below 75% of the ultimate strength.

The deformations in the specimens were monitored by installing strain gauges and linear variable differential transformers (LVDTs), as shown in Figure 8. Two LVDTs were used to measure the in-plane displacement at the top of the specimen and one LVDT was used to record the out-of-plane displacement of the wall. Strain gauges were attached on the top and bottom of the exterior parts of the steel channel sections at 674 mm and 60 mm above the base of the wall, respectively. The applied load was recorded using a load cell installed with the hydraulic jack during the experiment.

2. 4. Experimental Results and Discussion The key results from the experiment are listed in Table 2. The initial stiffness, ultimate load carrying capacity, ductility, failure mode and damage to the walls were the main parameters analyzed regarding the structural behavior of the specimens during the experiment. The ductility, measured in terms of displacement, was the ratio of the yield displacement to the ultimate displacement. The ultimate displacement was taken as the displacement

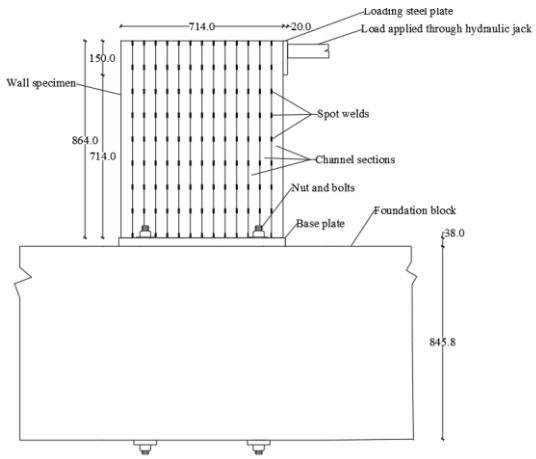

Figure 6. Experimental setup (all units in mm)

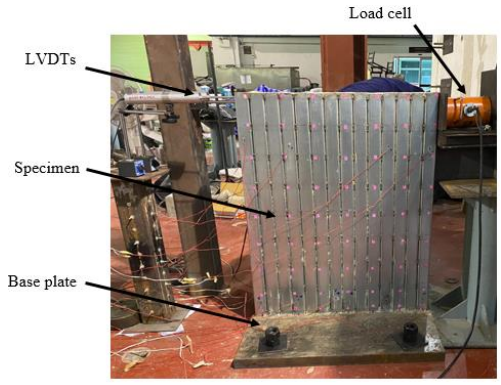

Figure 7. Actual setup in the laboratory

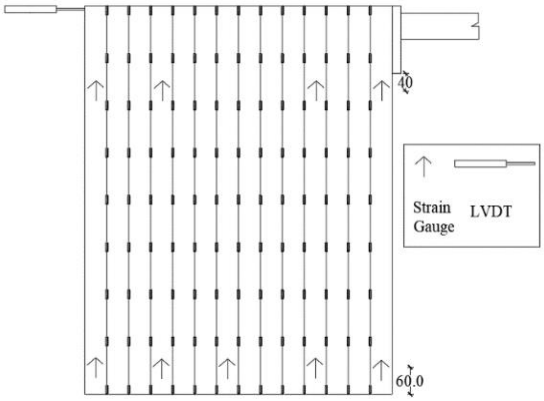

Figure 8. Instrumentation in specimen

corresponding to 85% of the ultimate load after the ultimate point [17]. As shown in Table 2, the initial stiffness of CFCSW2 was slightly higher than for CFCSW1 and CFCSW3, which was attributed to the flexibility of the foundation and base plate connection during the test.

2. 4. 1. Deformations in CFCSW1, CFCSW2 and CFCSW3 The curve shown in Figure 9 depicts that CFCSW1 failed in a brittle manner as the load displacement curve dropped suddenly immediately after reaching the ultimate loading stage. The first yielding of the specimen began at 227.7 kN as the steel at the bottom of the 1st channel (the 1st channel from the loading direction) started yielding in tension. Furthermore, the steel at the bottom of the 14th channel yielded at a load of 281.5 kN in compression. On further increasing the load, fracture of the steel at the base of the 1st channel occurred at almost the ultimate load. Finally, the specimen failed by the propagation of the steel fracture to the 2nd and 3rd channels and the buckling at the base of the 14th channel, as shown in Figure 10.

While, CFCSW2 showed relatively ductile failure mechanism. CFCSW2 first started yielding at a load of 346.3 kN in the 1st channel and at a load of 356.3 kN in 14th channel. Moreover, at approximately 80% of the ultimate load after the peak point, deformations (tearing and buckling of the steel near the welds) began to occur. Eventually, fracturing and buckling of the steel channels were noticed at approximately 75 % of the peak load (Figure 11). Whereas, CFCSW3 exhibited brittle failure, as demonstrated by the load displacement curve in Figure 7. CFCSW3 yielded for the first time when the load reached 230.0 kN. In addition, the nature and characteristics of the failure of the specimen was similar to CFCSW1 (Figure 12).

TABLE 2. Summary of test results

Specimen	Initial stiffness [kN/mm]	First yield load [kN]	Ultimate load [kN]	Ductility
CFCSW1	20.62	227.7	290.7	1.65
CFCSW2	22.76	346.3	378.0	1.87
CFCSW3	19.84	230.0	250.3	1.58

2. 4. 2. Comparisions Increasing the weld spacing shifted the failure mechanism from brittle failure, as noticed in CFCSW1, to ductile failure, as in CFCSW2.

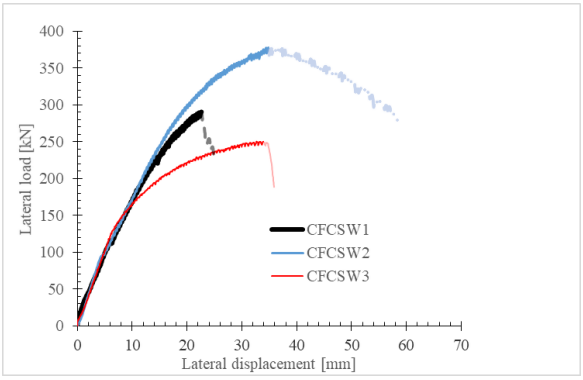

Figure 9. Lateral load displacement curve for CFCSW1, CFCSW2 and CFCSW3

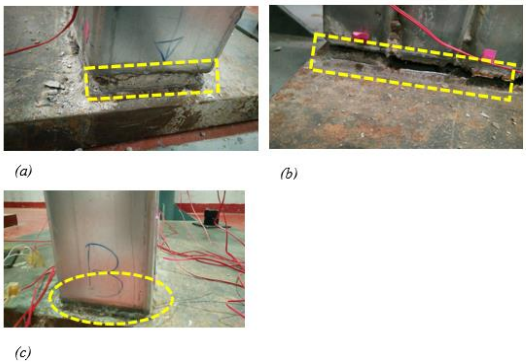

Figure 10. CFCSW1 (a) and (b), fracturing of steel and concrete cracking on tension side (c) buckling of steel on compression side

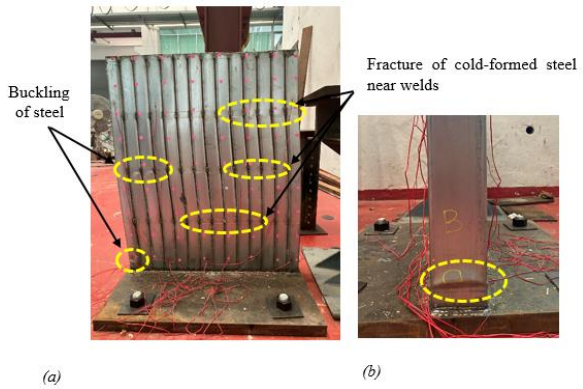

Figure 11. CFCSW2 (a) side view of damages (steel fracturing and buckling) (b) buckling of 14th channel

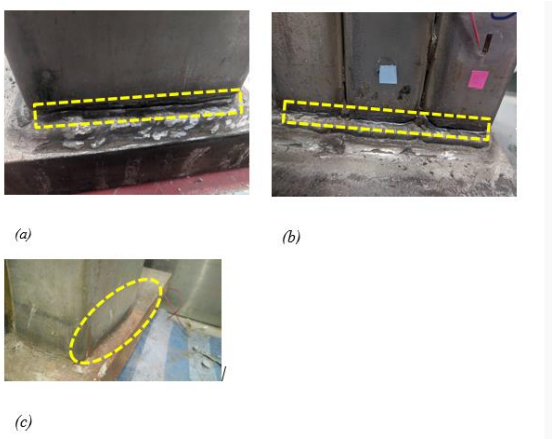

Figure 12. CFCSW3 (a) and (b), fracturing of steel at base of 1st, 2nd and 3rd channels (c) buckling of steel at base of 14th channel

The stiffness of CFCSW2 was slightly higher than for CFCSW1 prior to the first yield point, as demonstrated by curve in Figure 9. CFCSW1 and CFCSW2 yielded when the imposed loads were 227.7 kN and 325.7 kN, respectively, indicating a 52% increase in yield strength. The ultimate loads of CFCSW1 and CFCSW2 were 290.7 kN and 377.9 kN, respectively, representing a 30% improvement in ultimate capacity. The ductility ratios of CFCSW1 and CFCSW2 were 1.65 and 1.87, respectively, representing a 13% enhancement in ductility. The welds, in the form of spots, acted like rigid parts compared to the other remaining portions; consequently, column behavior was noticed between the spot welds. The heights of the column-like structures formed in CFCSW1 were about half of height of the columns in CFCSW2. Therefore, the columns in CFCSW1 behaved as short columns, which, when loaded laterally, failed by shear at the base in the experiment. In contrast, with CFCSW2, the height of the columns was sufficient to provide flexibility to the wall and thus there was ductile behavior in the experiment. Similarly, residual stresses were generated in the channel sections due to the welding. Hence, increasing the weld spacing from 105 mm to 211 mm decreased the amount of residual stress generated in the specimen which was the another reason for such manifestation.

The failure pattern of CFCSW2, with holes, was ductile in nature, whereas CFCSW3, without holes, failed in a brittle manner, which illustrated the effect of the web holes on failure. The load displacement curve showed that CFCSW2 had high stiffness relative to CFCSW3. The yield strength of CFCSW3 was 230.0 kN, which was a 33% decrease in yield strength compared to CFCSW2. Similarly, the load corresponding to the ultimate capacity was 250.3 kN for CFCSW3, which represented a 34% decrease in ultimate capacity. For CFCSW3, the ductility ratio was about 1.58, which was 15% less than for CFCSW2. The holes in the inner webs improved the structural behavior by two means. First, it provided ductility to the wall by acting as the weakest point in the wall. Consequently, the wall utilized the strength of the concrete and steel to a greater extend. Furthermore, the holes decreased the area of contact for friction between the steel and concrete. As a result, the integrity of the composite structure was enhanced.

3. FINITE ELEMENT MODELING

3. 1. Modeling Assumptions Non-linear finite element modeling of the specimens was conducted using the finite element software, ABAQUS. The 3-D model developed during the finite element modeling (FEM) is shown in Figure 13.

Eight-node solid elements (C3D8R) were used to model the filled concrete, base plate and loading plate. Similarly, the cold-formed channel sections were represented by four-node shell elements (S4R). Iterations with different mesh sizes were carried out to determine the optimum mesh size that did not compromise the output results, and at the same time, reduced the computation time.The filled concrete, base plate, and loading plate were meshed with a size of 20 mm x 20 mm x 20 mm. Similarly, 20 mm x 20 mm mesh was used for the steel channel sections. The welds connecting the channel sections were replicated by joining the nodes with point-based fasteners, as shown in Figure 13. Point-based fasteners are generally used to model the point-to-point connections between two or more surfaces and are independent of the mesh [25]. Surface-to-surface contact was used to represent the interaction between the concrete and steel, with hard contact attributed in the normal direction to prevent the penetration of slave nodes into the master segments, while frictional contact was assigned in a tangential direction [26]. Friction coefficient of 0.2 was used during the FEM by calibrating with the experimental results. The contact between the

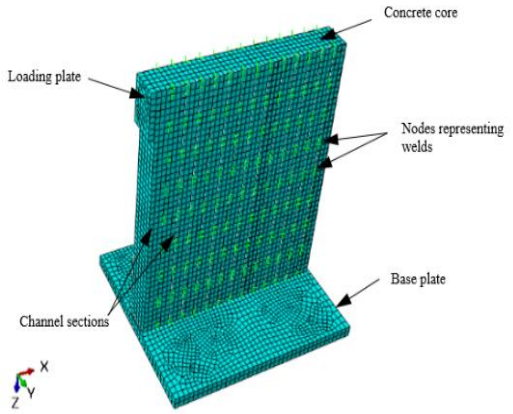

Figure 13. ABAQUS model of CFCSW

channel sections and the base plate was modeled by a surface-based shell-to-solid coupling constraint. Surface-based tie constraint was employed for simulating the contact behavior between the loading plate and the first channel section. Flexibility between the baseplate and foundation block was considered as in the experiment during the FEM. The force method was implemented for loading the steel plate.

3. 2. Material Modeling In this research, filled concrete was modeled using the concrete-damaged plasticity (CDP) model available in ABAQUS. The CDP model can be used when concrete is subjected to monotonic, cyclic and/or dynamic loading under low confining pressures (less than four or five times the uniaxial compressive strength of concrete) [27]. This model had been deployed in similar research to simulate the behavior of concrete [28-30]. The CDP model requires the input parameters such as the uniaxial tensile and compressive behavior, damage parameters, parameters to define the flow potential and yield surface and a viscosity parameter [27]. The plasticity parameters that were determined based on trails and used in the FEM are listed in Table 3, where F_{bo}/F_{co} is the ratio of initial equibiaxial compressive yield stress to initial uniaxial compressive yield stress and K is the ratio of the second stress invariant on the tensile meridian to that on the compressive meridian.

The stress-strain curve of concrete was used to model the uniaxial compressive behavior of the concrete (Figure 14(a)), with the ascending and descending branches of the curve defined by Equation (1), which was proposed by Popovics [31] and Equation (2), which was from Sanez [32], respectively. Nguyen and Whittaker [28] demonstrated that this approach was appropriate for such types of shear wall.

$$\sigma = f_c' \frac{k\left(\frac{\varepsilon}{\varepsilon_c}\right)}{1+(k-1)\left(\frac{\varepsilon}{\varepsilon_c}\right)^r} \quad (1)$$

$$\sigma = f_c' \frac{k\left(\frac{\varepsilon}{\varepsilon_c}\right)}{1+A\left(\frac{\varepsilon}{\varepsilon_c}\right)+B\left(\frac{\varepsilon}{\varepsilon_c}\right)^2+C\left(\frac{\varepsilon}{\varepsilon_c}\right)^3} \quad (2)$$

in which:

$$k=\frac{E_o\varepsilon_c}{f_c'}, \quad k_\varepsilon=\frac{\varepsilon_f}{\varepsilon_c}, \quad k_\sigma=\frac{f_c'}{f_f}, \quad r=\frac{k}{k-1},$$

$$A=C+k-2, \quad B=1-2C, \quad C=\frac{k(k_\sigma-1)}{(k_\varepsilon-1)^2}-\frac{1}{k_\varepsilon}$$

where E_o is the modulus of elasticity of concrete, f_c' is the compressive strength of concrete (21.0 MPa), ε_c is the strain corresponding to peak strength (0.002) and f_f and ε_f are stress and strain after the peak strength, which can be controlled by the user.

The concrete behavior in tension was represented by the linear stress-strain curve up to the peak strength and by the stress-crack width relationship after the peak point. Figure 14(b) shows stress-crack width relationship of concrete in tension computed as per the CEB-FIP model code 1990 [33], which includes the calculation of the tensile strength (f_t'), fracture energy (G_F), and crack width at which the tensile strength reduces to zero (w_o), using Equations (3), (4) and (5), respectively.

$$f_t' = 0.95\left(\frac{f_c'}{10}\right)^{2/3} \quad (3)$$

$$G_F = 0.025\left(\frac{8+f_c'}{10}\right)^{0.7} \quad (4)$$

$$w_o = 2\frac{G_F}{f_t'} \quad (5)$$

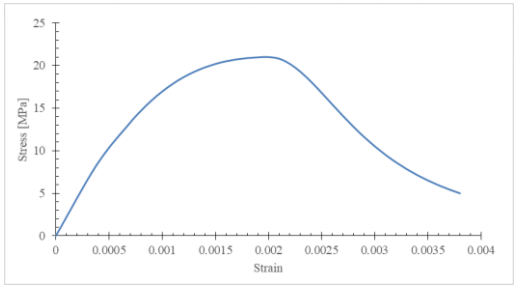

(a)

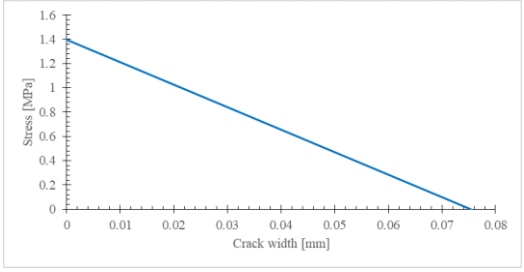

(b)

Figure 14. Stress-strain curve of concrete in: (a) Compression (b) Tension

The classical metal plasticity models in ABAQUS allows for the elastic perfectly plastic mod-eling of steel based on the Mises yield surfaces with associated plastic flow [27]. Therefore, steel during the FEM was modelled as elastic perfectly plastic, with the necessary parameters determined from the standard tensile coupon test.

3. 3. Validation of Finite Element Modeling Figure 15 and Table 4 represent the load displacement curves and ultimate load capacities, respectively, obtained from the FEM together with the experiment results. As shown, the ultimate capacities and overall behavior of the walls were reasonably predicted by the FEMs. Furthermore, the buckling modes of 14th channel (Figure 16) verified that deformations were similar in the FEM and the experiment. The slight difference in the response between the FEM and the test could have been due to the approximations of actual materials in the FEM, selection of the material constitutive models and imperfections in the geometry.

3. 4. Parametric Study The benchmarked FEM was further used to conduct the parametric studies to investigate the effect of different parameters on the lateral load capacity of CFCSW. CFCSW2 was selected to carry out the parametric investigation, where the variables were: the weld spacing, steel thickness, concrete thickness and the height of the wall. Table 5 presents the details of the walls with their respective

TABLE 3. Plasticity parameters

Dilation Angle	Eccentricity	F_{b0}/F_{c0}	K
20	0.1	1.10	0.67

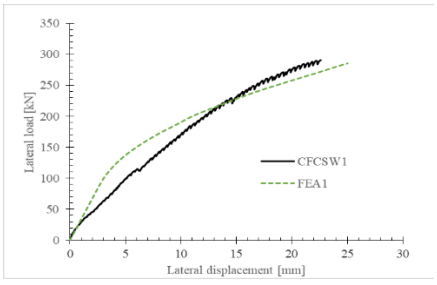

(a)

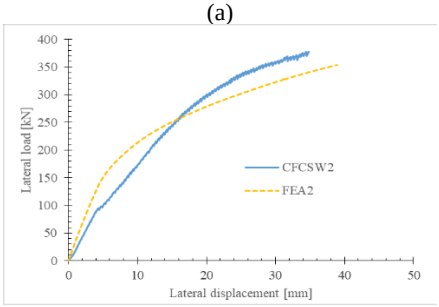

(b)

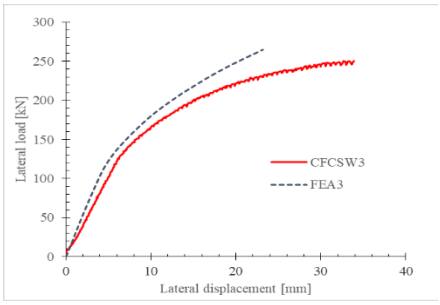

(c)

Figure 15. Comparison of load displacement curves between experiment and FEM: (a) CFCSW1 (b) CFCSW2 (c) CFCSW3

TABLE 4. Comparisions between test and FEM results

Specimen	Experimental results	FEM results	(1)/(2)
	(1) Ultimate load (kN)	(2) Ultimate load (kN)	
CFCSW1	290.6	285.4	1.02
CFCSW2	378	354.1	1.06
CFCSW3	250.3	265.1	0.95

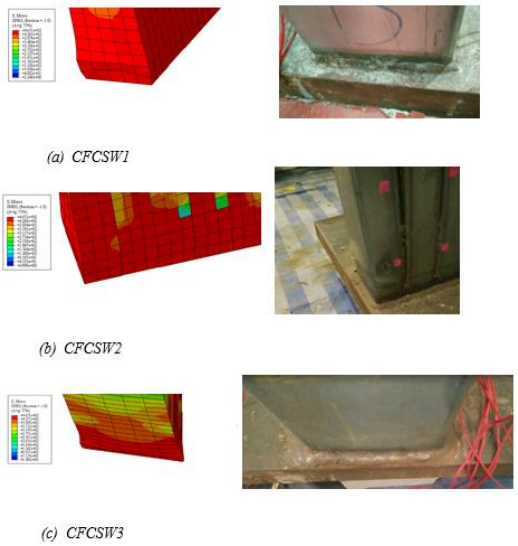

Figure 16. Buckling of last channel during FEM and in test for: (a) CFCSW1 (b) CFCSW2 (c) CFCSW3

ultimate capacities maintaining constant values for the other parameters (concrete strength, steel strength and hole size) for all analyses, except for CFCSW2 with a concrete thickness of 50 mm (CFCSW2-T50), where a hole size of 40 x 80 mm was used. Figure 17 depicts the responses of CFCSWs for different varied parameters.

3. 4. 1. Effect of Weld Spacing Weld spacing (center to center) in the wall was varied while keeping

TABLE 5. Details of variables with obtained ultimate load

Test specimen	Clear Height (h) (mm)	Length(l) (mm)	Aspect ratio (h/l)	Weld spacing (mm)	Steel thickness (mm)	Concrete thickness (mm)	Ultimate load (kN)
CFCSW2	714	714	1	211	1.5	99	354.10
CFCSW2-WS105	714	714	1	105	1.5	99	285.44
CFCSW2-WS141	714	714	1	141	1.5	99	315.52
CFCSW2-WS281	714	714	1	281	1.5	99	311.15
CFCSW2-WS422	714	714	1	422	1.5	99	216.35
CFCSW2-t1	714	714	1	211	1	99	254.31
CFCSW2-t2	714	714	1	211	2	99	440.72
CFCSW2-t2.5	714	714	1	211	2.5	99	512.20
CFCSW2-T50	714	714	1	211	1.5	50	294.52
CFCSW2-T150	714	714	1	211	1.5	150	381.84
CFCSW2-T200	714	714	1	211	1.5	200	403.47
CFCSW2-H971	971	714	1.36	211	1.5	99	249.01
CFCSW2-H827	827	714	1.16	211	1.5	99	303.32
CFCSW2-H642	642	714	0.9	211	1.5	99	385.70

The suffix after the CFCSW2 represents the changed variables: for example, WS105, t1, T50 and H827 indicate the wall with weld spacing 105 mm, steel channel thickness 1 mm, concrete thickness 50 mm and height 827 mm, respectively.

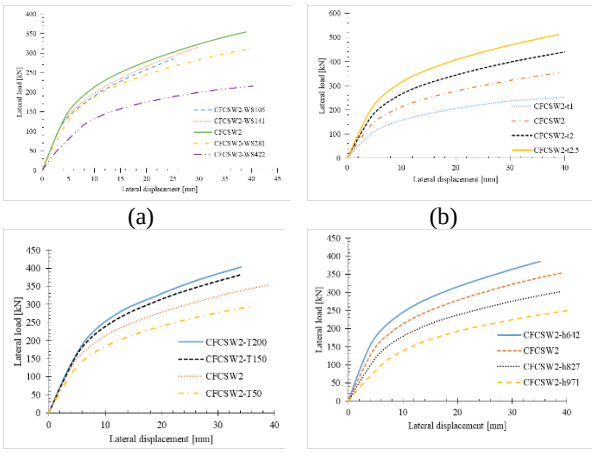

(a) (b) (c) (d)

Figure 17. Load displacement curves for different parameters: (a) weld spacings (b) steel channel thicknesses (c) concrete thicknesses (d) heights

other parameters constant to determine its effect on the ultimate capacity. The load displacement curves for different weld spacings are illustrated in Figure 17(a). Figure 18 represents the deformations of the finite element models showing the yielding of steel, represented by the red color, and the cracking and crushing of concrete at the ultimate load. Decreasing the weld spacing from 211 mm to 141 mm and to 105 mm had an adverse effects on the stiffness, ductility, and ultimate load of the wall, which decreased the ultimate load by 11 % and 19 %, respectively. Likewise, when the weld spacing was increased from 211 mm to 281 mm and to 422 mm, the ultimate capacity of the wall decreased by 12 % and 38%, respectively, and stiffness of the wall also decreased (Figure 17(a)). When the weld spacing of the wall decreased from 211 mm to 141 mm and to 105 mm, each channel section became stiffer due to its increasing unity of overall structure. However, the increase in stiffness also resulted in the concentration of stresses at specific location, and thus, the redistribution of the applied load did not happen effectively in the model till its peak load stage. This phenomenon caused the premature cracking and crushing of concrete (Figure 18(b)) and the non-uniform yielding of steel channel sections in the wall (Figure 18(a)). Similarly, increasing the weld spacing from 211 mm to 281 mm and to 422 mm loosened the integrity of the structure. So, the overall strength of materials throughout the wall was not used effectively as shown in Figures 18(e) and 18(f), where less yielded steel and smaller values of maximum principle plastic strains can be observed comparing to ones in CFCSW2 (Figures 18(c) and 18(d)). Thus, both increasing and decreasing the weld spacing from 211 mm reduced the ultimate load carrying capacity of the CFCSW.

3. 4. 2. Effect of Steel Channel Thickness The load displacement curves with different steel thicknesses are presented in Figure 17(b). The peak strength increased by 24% and 44% with increases in the steel

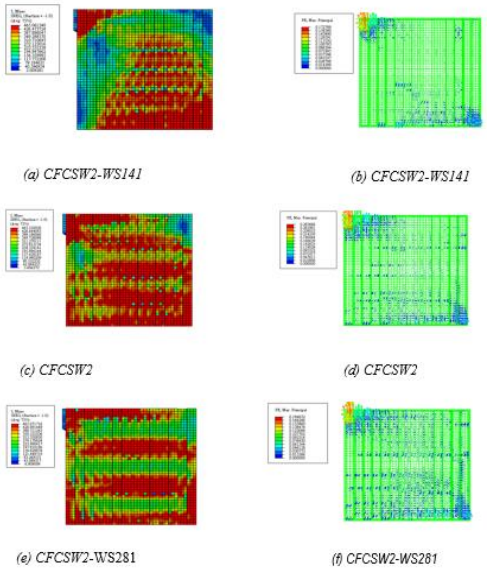

Figure 18. Yielded cold formed steel, and cracked and crushed filled concrete at ultimate load: (a) CFCSW2-WS141- steel deformation (b) CFCSW2-WS141- concrete deformation (c) CFCSW2-steel deformation (d) CFCSW2-concrete deformation (e) CFCSW2-WS281- steel deformation (f) CFCSW2-WS281-concrete deformation

thickness from 1.5 mm to 2 mm and to 2.5 mm, respectively, whereas the load capacity decreased by 28% when the steel thickness changed from 1.5 mm to 1 mm. In other words, the direct relationship between the steel thickness and ultimate capacity of CFCSW was observed.

3. 4. 3. Effect of Concrete Thickness The filled concrete thickness, whose value is equal to the inner length of the web of the steel channel, was differed while the other parameters remained unchanged. Figure 17(c) illustrates the load displacement curves obtained from the analysis for different concrete thicknesses. Increasing the concrete thickness from 99 mm to 150 mm and to 200 mm improved the capacity by 7.8% and 20%, respectively, while decreasing concrete thickness from 99 mm to 50 mm reduced the ultimate capacity by 16 %. Therefore, the stiffness and ultimate capacity of CFCSW was proportional to the concrete thickness.

3. 4. 4. Effect of Height The responses in terms of load displacement curves are shown in Figure 17(d). When the height of the wall was changed from 714 mm to 827 mm and to 971 mm with aspect ratio of 1.16 and 1.36, respectively, the load bearing capacity of the wall was reduced by 14% and 30%, respectively. Similarly, the stiffness of the wall decreased with an increase in height. The peak load and stiffness of the wall both increased with reduction in height from 714 mm to 642 mm. Therefore, with an increase in height, peak strength and stiffness of the CFCSW decreased, while with a reduction in height, the strength and stiffness improved.

3. 4. 5. Sensitivity Analysis The responses of the different CFCSW setups in terms of ultimate load capacity were analysed to determine the sensitivity of load carrying capacity of the CFCSWs to the different parameters that were altered in the parametric analysis. Figure 19 shows the sensitivity analysis of the peak strength of the CFCSWs to the parameters of weld spacing, steel plate thickness, height and concrete thickness. As depicted in Figure 17, V_u/V_u' denotes the normalized values, where V_u represents the ultimate load capacity of the CFCSWs with changed variables, while V_u' is the load capacity of CFCSW2, which was taken as mean value for comparison. Likewise, X/X' on the x-axis also indicates the normalized values of the parameters and was obtained using correlation with the parameters of CFCSW2. It can be seen in Figure 19 that the absolute change in the peak strength of the CFCSWs with the change in height was higher than for the other parameters, as the curve corresponding to the height effect was stiffer than the others. In summary, the parameters can be arranged in the following order based on maximum to minimum impact on the load carrying capacity of CFCSW: height, steel plate thickness, weld spacing and concrete thickness.

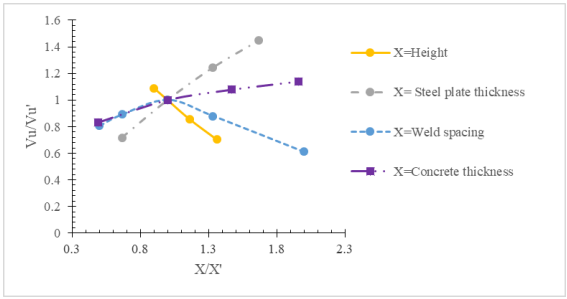

Figure 19. Sensitivity analysis of parameters on load carrying capacity of CFCSW

4. CONCLUSIONS

The following conclusions were made from this investigation:

1. Increasing the weld spacing from 105 mm to 211 mm increased the load carrying capacity by 30% and improved the stiffness and ductility of the different CFCSW types tested.
2. Providing holes inside the specimen on the web of the channel sections improved the peak strength by 50% with increase in the stiffness and ductility of the different CFCSW types tested.
3. The failure mode of the CFCSW changed from brittle mode to ductile mode with an increase in the weld

spacing from 105 mm to 211 mm as demonstrated by CFCSW1 and CFCSW2, respectively, or with the provision of holes inside the specimen as illustrated by CFCSW2 and CFCSW3, respectively.

4. Non-linear FEM was used and validated with the experimental results based on the ABAQUS modeling, and the FEMs simulated the overall behavior and satisfactorily predicted the load carrying capacity of the CFCSW.

5. Parametric studies were conducted on the benchmarked models and indicated that increasing the weld spacing from 105 mm to 211 mm increased the stiffness, ductility, and ultimate capacity, while further increasing the weld spacing from 211 mm to 422 mm decreased the stiffness and ultimate capacity of the CFCSW. Similarly, the stiffness and load carrying capacity of the CFCSW decreased with an increasing height of the wall, whereas decreasing the height improved the stiffness and capacity. Increasing the steel and concrete thickness enhanced the stiffness and peak strength of the CFCSW and vice versa.

6. The results from the sensitivity analysis illustrated that the ultimate capacity of the CFCSW was most sensitive to the effect of height, while it was least sensitive to the effect of concrete thickness.

5. REFERENCES

1. Zhang, W., Wang, K., Chen, Y., Ding, Y., "Experimental study on the seismic behaviour of composite shear walls with stiffened steel plates and infilled concrete", ***Thin-Walled Structures,*** Vol. 144, (2019). DOI: 10.1016/j.tws.2019.106279
2. Zhang, X., Qin, Y., Chen, Z., "Experimental seismic behavior of innovative composite shear walls", ***Journal of Constructional Steel Research***, Vol. 116, (2016), 218-232. DOI: 10.1016/j.jcsr.2015.09.015
3. Pavel, F., Panfilii, P., Farangsi, E. N., "Estimation of displacement capacity of rectangular RC shear walls using experimental and analytical database", ***Civil Engineering Journal***, Vol. 3, (2020). DOI: 10.14311/CEJ.2020.03.0035
4. Honarmand, S., Homami, P., Gharehbaghi, V., Farangsi, E. N., "A study on the significance of the design parameters of steel plate shear walls subjected to monotonic loading", ***Civil and Environmental Engineering Reports***, Vol. 30, (2020), 0142-0154. DOI: 10.2478/ceer-2020-0056
5. Berman, J. W., "Seismic behavior of code designed steel plate shear walls", ***Engineering Structures***, Vol. 33, (2011), 230-244. DOI: 10.1016/J.ENGSTRUCT.2010.10.015
6. Guo, L., Li, R., Zhang, S., Yan, G., "Hysteretic analysis of steel plate shear walls (SPSWs) and a modified strip model for SPSWs", ***Advances in Structural Engineering***, Vol. 15, (2012), 1751-1764. DOI: 10.1260/1369-4332.15.10.1751
7. Nie, J., Zhu, L., Fan, J., Mo, Y., "Lateral resistance capacity of stiffened steel plate shear walls", ***Thin-Walled Structures***, Vol. 67, (2013), 155-167. DOI: 10.1016/j.tws.2013.01.014
8. Chen, G., Guo Y., Fan Z., Han, Y., "Cyclic test of steel plate shear walls", ***Journal of Building Structures***, Vol. 25, (2004), 19-26. http://en.cnki.com.cn/Article_en/CJFDTOTAL-JZJB200402003.htm
9. Guo, L., Li, R., Rong, Q., Zhang, S., "Cyclic behavior of SPSW and CSPSW in composite frame", ***Thin-Walled Structures***, Vol. 51, (2012), 39-52. DOI: 10.1016/j.tws.2011.10.014
10. Guo, L., Rong, Q., Qu, B., Liu, J., "Testing of steel plate shear walls with composite columns and infill plates connected to beams only", ***Engineering Structures***, Vol. 136, (2017), 165-179. DOI: 10.1016/j.engstruct.2017.01.027
11. Liao, F., Han, L., Tao, Z., "Seismic behaviour of circular CFST columns and RC shear wall mixed structures: Experiments", ***Journal of Constructional Steel Research***, Vol. 65, (2009), 1582-1596. DOI: 10.1016/j.jcsr.2009.04.023
12. Munesi, A., Sharbatdar, M., Gholhaki, M., "An investigation into the factors influencing the cyclic behavior of the buckling-restrained steel plate shear walls", ***Steel construction***, Vol. 14, (2020). DOI: 10.1002/stco.201900047
13. Dan, D., fabian, A., Stoian, V., "Theoretical and experimental study on composite steel–concrete shear walls with vertical steel encased profiles", ***Journal of Constructional Steel Research***, Vol. 67, (2011), 800-813. DOI: 10.1016/j.jcsr.2010.12.013
14. Lu, X., Gan, C., Wang, W., "Study on seismic behavior of steel plate reinforced concrete shear walls", ***Journal of Building Structures***, Vol. 30, (2009), 89-96. http://www.jzjgxb.com/EN/Y2009/V30/I05/89
15. Vecchio, F. J., McQuade, I., "Towards improved modeling of steel-concrete composite wall elements", ***Nuclear Engineering and Design***, Vol. 241, (2011), 2629-2642. DOI: 10.1016/j.nucengdes.2011.04.006
16. Zhao, Q., Astaneh, A., "Cyclic Behavior of Traditional and Innovative Composite Shear Walls", ***Journal of Structural Engineering***, Vol. 130, (2003), 271-284. DOI: 10.1061/(ASCE)0733-9445(2004)130:2(271)
17. Luo, Y., Guo, X., Li, J., Xiong, Z., Meng, L., Dong N. Zhang, J., "Experimental Research on Seismic Behaviour of the Concrete-Filled Double-Steel-Plate Composite Wall", ***Advances in Structural Engineering***, Vol. 18, (2016), 1845-1858. DOI: 10.1260/1369-4332.18.11.1845
18. Ozaki, M., Akita, S., Osuga, H., Nakayama, T., Adachi, N., "Study on steel plate reinforced concrete panels subjected to cyclic in-plane shear", ***Nuclear Engineering and Design***, Vol. 228, (2004), 225-244. DOI: 10.1016/j.nucengdes.2003.06.010
19. Varma, A. H., Malushte, S. R., Sener, K. C., Lia, Z., "Steel-plate composite (SC) walls for safety related nuclear facilities: Design for in-plane forces and out-of-plane moments", ***Nuclear Engineering and Design***, Vol. 269, (2014), 240-249. DOI: 10.1016/j.nucengdes.2013.09.019
20. Booth, P. N., Bhardwaj, S. R., Tseng, T., Seo, J., Varma, A. H., "Ultimate shear strength of steel-plate composite (SC) walls with boundary elements", ***Journal of Constructional Steel Research***, Vol. 165, (2020). DOI: 10.1016/j.jcsr.2019.105810
21. Epackachi, S., Nguyen, N. H., Kurt, E. G., Whittaker, A. S., Varma, A. H., "In-Plane Seismic Behavior of Rectangular Steel-Plate Composite Wall Piers", ***Journal of Structural Engineering***, (2014). DOI: 10.1061/(ASCE) ST.1943-541X.0001148
22. AWS D1.3/D1.3M:2018, "Structural welding code- Sheet steel", (2018).
23. AISI S100-16w/S1-18, "North American specification for the design of cold-formed steel structure members", (2016).
24. AISC design guide 31, "Castellated and cellular beam design", (2016).
25. ABAQUS 6.14, "Abaqus analysis user's guide- Volume IV: Elements", (2014).
26. ABAQUS 6.14, "Abaqus analysis user's guide- Volume V: Prescribed conditions, constraints and interactions", (2014).

27. ABAQUS 6.14, "Abaqus analysis user's guide- Volume III: Materials", (2014).
28. Nguyen, N. H., Whittaker, A. S., "Numerical modelling of steel-plate concrete composite shear walls", ***Engineering Structures***, Vol. 150, (2017), 1-11. DOI: 10.1016/j.engstruct.2017.06.030
29. Epackachi, S., Whittaker, A. S., "Experimental, numerical and analytical studies on the seismic response of steel-plate concrete (SC) composite shear walls", ***Earthquake Engineering to Extreme Events***, (2016). http://www.buffalo.edu/mceer/catalog.host.html/content/shared/www/mceer/publications/MCEER-16-0001.detail.html
30. Rahmani, Z., Naghipour, M., Nematzadeh, M., "Flexural performance of high-strength prestressed concrete-encased concrete-filled steel tube sections", ***International Journal of Engineering, Transactions C: Aspects***, Vol. 32, No. 9, (2019), 1238-1247. DOI: 10.5829/ije.2019.32.09c.03
31. Popovics, S., "A numerical approach to the complete stress-strain curve of concrete", ***Cement and Concrete Research***, Vol. 3, (1973), 583-599. https://doi.org/10.1016/0008-8846(73)90096-3
32. Sanez, L. P., "Discussion of equation for the stress-strain curve of Concrete, by Desayi P. and Krishnan S", ***ACI Journal***, Vol. 61, (1973), 1227-1239.
33. CEB-FIP model code 1990, "Design code", (1990).

Persian Abstract

چکیده

نوع جدیدی از دیوارهای برشی کامپوزیتی نوآورانه ، دیوار برشی فولادی شکل سرد پر شده با بتن (CFCSW)پیشنهاد شده است ، که از بخشهای کانال سرد تشکیل شده و به طول ۲۰ میلی متر جوش داده شده و با بتن پر شده است. مطالعه اصلی CFCSW بر رفتار کلی ، ظرفیت بار نهایی ، سفتی و شکل پذیری تمرکز دارد. سه نمونه از CFCSW با نسبت تصویر ۱.۰ تحت بار یکنواخت جانبی آزمایش می شوند. مدلهای اجزای محدود سه بعدی با نتایج تجربی توسعه داده شده و معیار قرار می گیرند. مدلهای معتبر برای انجام مطالعات پارامتریک برای تعیین تأثیر پارامترها بر عملکرد CFCSW استفاده می شوند. پارامترها عبارتند از ارتفاع ، ضخامت ورق فولادی ، فاصله جوش و ضخامت بتن .CFCSWنتایج مدل سازی عناصر تجربی و محدود نشان می دهد که افزایش فاصله جوش از ۱۰۵ میلی متر به ۲۱۱ میلی متر ، سخت ، شکل پذیری و ظرفیت حمل بار را بهبود می بخشد و به طور مشابه ، ایجاد سوراخ در داخل دیوار باعث افزایش سختی ، شکل پذیری و استحکام CFCSW می شود. ظرفیت نهایی CFCSW بیشترین تأثیر را بر تغییر ارتفاع دیوار می گذارد و کمترین آن را متغیر بودن ضخامت بتن دیوار می کند.